Cross-section ratio of double to single ionization of helium by Compton scattering of 40–100-keV x rays

L. Spielberger,[1,*] H. Bräuning,[2,1] A. Muthig,[1] J. Z. Tang,[3] J. Wang,[4] Y. Qiu,[3] R. Dörner,[1] O. Jagutzki,[1] Th. Tschentscher,[5] V. Honkimäki,[5] V. Mergel,[1] M. Achler,[1] Th. Weber,[1] Kh. Khayyat,[1] J. Burgdörfer,[3,6] J. McGuire,[4] and H. Schmidt-Böcking[1]

[1]*Institut für Kernphysik, Universität Frankfurt, August-Euler-Straße 6, D-60486 Frankfurt, Germany*

[2]*Department of Physics, Kansas State University, Manhattan, Kansas 66506*

[3]*Department of Physics, University of Tennessee, Knoxville, Tennessee 37996-1200 and Oak Ridge National Laboratory, Oak Ridge, Tennessee 37831-6377*

[4]*Department of Physics, Tulane University, New Orleans, Louisiana 70118-5698*

[5]*European Synchrotron Radiation Facility, 38043 Grenoble, France*

[6]*Institute for Theoretical Physics, Vienna University of Technology, Wiedner Hauptstraße 8-10, A 1040 Vienna, Austria*

(Received 20 August 1998)

We have measured the ratio of cross sections for double to single ionization of helium by Compton scattering, $R_C=\sigma_C^{++}/\sigma_C^{+}$, at photon energies of 40, 80, and 100 keV using cold target recoil-ion momentum spectroscopy. Comparison with calculations involving highly correlated initial states and approximate final states with and without final-state correlations, represented by $3C$ and $2C$ wave functions respectively, shows that the influence of final-state correlations persists to very high photon energies. A comparison with recent charged-particle data is made. [S1050-2947(99)04701-0]

PACS number(s): 32.80.Cy, 31.25.−v, 39.30.+w

I. INTRODUCTION

Double ionization in high-energy collisions of atoms with both photons and charged particles is predominantly caused by the electron-electron interaction occurring during these collisions. In describing the many-body dynamics of this process [1], the photon-induced double ionization of helium still provides a challenging task. Already the integrated probability for double ionization, expressed by the ratio of total cross sections for double to single ionization, $R=\sigma^{++}/\sigma^{+}$, can therefore serve as a tool to investigate the properties of bound and continuum wave functions as well as of the collision process itself. Of particular interest is the behavior at high photon energies for which R is expected to approach an asymptotic limit and detailed tests of the influence of many-body correlations in the initial ground states and in continuum final states should become possible.

For photoabsorption, which is the dominant process below a photon energy of around 6 keV, early calculations predicted an asymptotic value of R_{ph}^{∞} close to 1.7%, which recently has been experimentally confirmed [2–5]. In addition, fully *ab initio* calculations for photon energies from threshold to asymptotically high energies have now become available [6]. For Compton scattering, on the other hand, the situation is less clear. A theoretical calculation for double ionization by Compton scattering [7] indicated that the ratio R_C should lie below the ratio for photon absorption. Detailed investigations of the nonrelativistic high-energy limit yielded a theoretical value of $\approx 0.84\%$ [8–10], which is, with one exception [11], generally agreed on as the asymptotic value. Experimentally, the high-energy behavior for double ionization by Compton scattering has not yet been firmly established. Specifically, recent observations of the ratio R_C remain in conflict. At incident photon energies between 40 and 120 keV observed values of R_C differ, ranging from 0.8% to 1.3% with errors smaller than the differences in the mean values. Moreover, the most recent observation of Becker *et al.* [12] seems to indicate that R_C is still decreasing with increasing photon energy at 120 keV.

One model for Compton scattering at high photon energies is based on the so-called ''sudden approximation'' [3]. In this case one electron is treated to be removed instantaneously and final-state interactions are neglected so that the probability for double ionization mainly depends on the overlap matrix element of the initial atomic ground state with a continuum state of the ionized atom. Therefore in this model the probability for double ionization is proportional to the one of single ionization. In contrast to photoabsorption, which probes only certain parts of the electron wave function, the removal of the first electron via Compton scattering does not depend on its actual momentum or position. As a consequence, any sudden process that fulfills the condition of a nonselective probing of the electron wave function, namely, high-energy Compton scattering and ionization from fast charged particles with high-energy transfer, should result in one common value of R [13].

In the present paper we investigate both experimentally and theoretically the high-energy behavior of double ionization by Compton scattering in the photon energy range between 40 and 100 keV. We focus on questions as to what the experimental value of R_C is and how quickly the asymptotic regime is reached. We present an experimental investigation of R_C in an extended high-energy regime at 40, 80, and 100 keV together with calculations of R_C as a function of E_γ up to 100 keV. The experiments were performed with the

*Electronic address: spielberger@ikf.uni-frankfurt.de

 ©1999 The American Physical Society

COLTRIMS (cold target recoil-ion momentum spectroscopy) method [14], which provides for a unique control over the commonly discussed sources of possible errors in a measurement of R [15,16]. In this work parallel measurements were performed with independent spectrometers and detectors to achieve a new quality of precision with respect to systematical errors. We observe small but significant deviations from the asymptotic value $R_C^{\infty}\approx 0.84\%$. We interpret this as indications of the persistence of the influence of final-state correlations up to high photon energies. We will also compare our results with recent data for charged-particle collisions.

II. THEORY

We consider a helium atom interacting with a photon with the Hamiltonian

$$H=\sum_{j=1,2}\left(\frac{(\vec{p}_j+\vec{A}/c)^2}{2}+Z_T/r_j\right)+1/r_{12}. \tag{1}$$

Quantum mechanically, since Compton scattering involves both an incoming and an outgoing photon, the lowest order matrix element comes from the A^2 term in Eq. (1). For resonant Compton or resonant Raman scattering which occurs at photon energies close to the resonance energy of a bound transition, the $(\vec{p}\cdot\vec{A})^2$ term is dominant. At high energies well above resonances the A^2 term provides the leading contribution.

The Compton scattering cross section for inelastic scattering from an arbitrary initial state $|i\rangle$ to an arbitrary final state $|f\rangle$ may be expressed in first order as [17–19]

$$\left(\frac{d^2\sigma}{d\epsilon dQ^2}\right)_C=\frac{\pi r_0^2}{2k^2}\left[1+\left(1-\frac{Q^2}{2k^2}\right)^2\right]F_I(\epsilon,Q^2), \tag{2}$$

with

$$F_I(\epsilon,Q^2)=\int d\Omega\sqrt{2(\epsilon+\epsilon_i)}\left|\left\langle f\left|\sum_{j=1}^{N}e^{iQr_j}\right|i\right\rangle\right|^2 \tag{3}$$

the inelastic transition form factor (proportional to the generalized oscillator strength [19]) for the N-electron atom integrated over all emission angles of the emitted electron (Ω) and weighted with the density of continuum final states. In the case of multiple ionization, F_I is understood to include an integral over emission angles of all electrons and the proper density of states. r_0 is the classical electron radius [$r_0=(1/137)^2\ a.u.$], $\vec{Q}=\vec{k}_i-\vec{k}_f$ the momentum transfer by the Compton scattered photon, and $\epsilon_{i,f}$ the energy of the atomic initial (final) state.

For the initial state we use a correlated Hylleraas state of the form

$$\psi_i(\vec{r}_1,\vec{r}_2)=e^{-\sigma(r_1+r_2)/2}\sum_{n,j,k}C_{n,j,k}\sigma^{n+j+k}(r_1+r_2)^j \times j(r_1-r_2)^k r_{12}^n, \tag{4}$$

where n is integer, k even, and j both integer and half integer. The use of fractional powers allows us to conveniently approximate the effect of the logarithmic Fock singularity [20]. With 34 terms and variations of the coefficients C and σ we obtain the ground state energy $E_i=-2.903\,721$ a.u. compared to the Pekeris value [21] of $-2.903\,724$ a.u.

The primary difficulty lies in expressing correlation in the final-state wave function. For the latter we choose two different approximations: (a) a $2C$ final state

$$\psi_f^{2C}(\vec{r}_1,\vec{r}_2)=\frac{1}{\sqrt{2}}[\phi_{\vec{k}_1}^{(-)}(\vec{r}_1)\phi_{\vec{k}_2}^{(-)}(\vec{r}_2)+\phi_{\vec{k}_2}^{(-)}(\vec{r}_1)\phi_{\vec{k}_1}^{(-)}(\vec{r}_2)], \tag{5}$$

with

$$\phi_{\vec{k}}^{(-)}(\vec{r})=\frac{1}{(2\pi)^{3/2}}e^{\pi\eta/2}\Gamma(1+i\eta)e^{i\vec{k}\cdot\vec{r}} \times {}_1F_1[-i\eta,1,-i(kr+\vec{k}\cdot\vec{r})], \tag{6}$$

consisting of two incoming Coulomb waves and (b) a $3C$ final-state wave function containing the Coulomb distortion factor for the electron-electron repulsion,

$$\psi_f^{3C}(\vec{r}_1,\vec{r}_2)=\psi_f^{2C}(\vec{r}_1,\vec{r}_2)D^{(-)}(\vec{k}_{12},\vec{r}_{12}), \tag{7}$$

with

$$D^{(-)}(\vec{k}_{12},\vec{r}_{12})=e^{-\eta_{12}\pi/2}\Gamma(1-i\eta_{12}) \times {}_1F_1[i\eta;1;i(k_{12}r_{12}+\vec{k}_{12}\vec{r}_{12})] \tag{8}$$

and $\eta_{12}=1/(2k_{12})$.

While the $2C$ function does not contain final-state correlations (apart from the Pauli correlations due to the antisymmetrization), the $3C$ function contains Coulomb electron-electron correlations, albeit in a very approximate form. The standard justification for the usage of the $3C$ function relies on the fact that it satisfies the proper asymptotic boundary conditions for the Coulomb interacting particles [22,23] at large distances. For evaluating the matrix elements [Eq. (2)] this is, however, of little relevance since the localized initial state effectively cuts off the spatial integrations for $r\gg\langle r\rangle_i$ and renders therefore the matrix elements to be rather insensitive to the behavior of the wave functions at large distances. Our use of the $3C$ function relies on its behavior for asymmetric energy sharing $1/k_{12}\ll 1$ at large energy transfers, ΔE, for which it constitutes the satisfactory representation of the final-state correlations at small to intermediate interparticle distances. We have recently shown that for photoabsorption above photon energies of ≈ 1 keV, the $3C$ function is reasonably accurate because it is the proper leading order perturbative solution to the correlation problem for large energy transfers $\Delta E_{\rm ph}=\hbar\omega$ [6]. In the present case of Compton scattering at high photon energies the justification is less obvious. Unlike for photoabsorption, the energy transfer in Compton scattering, ΔE_C, is much smaller than $\hbar\omega$. The energy transfer by Compton scattering lies in the energy interval

$$0\leqslant\Delta E_C\leqslant E_{\rm BE}, \tag{9}$$

where $E_{\rm BE}$ denotes the binary-encounter (or backscattering) limit

$$E_{\mathrm{BE}}=\hbar\omega\,\frac{1}{1+mc^2/(2\,\hbar\omega)}. \tag{10}$$

For primary photon energies of $\approx$100 keV, $E_{\mathrm{BE}}\approx$28 keV. The energy differential cross section is only weakly dependent on ΔE_C for $\Delta E_C<\Delta E_{\mathrm{BE}}$, while it falls off precipitously in the region of $\Delta E_C>E_{\mathrm{BE}}$, which is forbidden within two-body kinematics. For energy transfers beyond this binary-encounter limit, Compton scattering probes high momentum components of the initial-state function [24], very much like for photoabsorption. With increasing photon energies, an increasing fraction of the energy transfers contributing to Compton scattering lies within the range of validity of the $3C$ approach. For example, at $\hbar\omega=100$ keV about 90% of the cross section originates from energy transfers above 1 keV. Nevertheless, even at such high energies a remaining fraction of $\leqslant$10% corresponds to low-energy transfers outside the validity of the $3C$ approach. This poses an intrinsic limit on the accuracy of the cross section and, hence, on the resulting ratio R_C.

Since for Compton scattering an increasingly large number of partial waves for the Compton scattered primary electron, l_1, contribute, the evaluation of the double ionization cross section using the $3C$ final state poses a considerable challenge. In our previous calculations [8], the distortion factor was taken into account only for the lowest partial waves $l_1=0,1,2$ where electron-electron correlation effects are presumed to be most important, while for higher partial waves only uncorrelated Coulomb waves were used. We have now implemented an evaluation procedure which permits the inclusion of the distortion factor for arbitrary high partial waves. Briefly, we use for $D^{(-)}$ the integral representation

$$\begin{aligned}D(\vec{k}_{12},\vec{r}_{12})=&\frac{\exp(-\pi\eta_{12}/2)}{\Gamma(i\eta_{12})}\\&\times\int_0^1\exp[-it(k_{12}r_{12}+\vec{k}_{12}\cdot\vec{r}_{12})]\\&\times t^{i\eta_{12}-1}(1-t)^{-i\eta_{12}}dt.\end{aligned} \tag{11}$$

Upon expansion of the plane wave factor

$$\exp(-it\vec{k}_{12}\cdot\vec{r}_{12})=\sum_l\,(2l+1)(-i)^l j_l(ts_{12})P_l(\gamma_{12}), \tag{12}$$

where we use $\gamma_{12}=\cos\theta_{\hat{k}_{12}\cdot\hat{r}_{12}}$ and $s_{12}=k_{12}r_{12}$, the partial-wave expansion becomes

$$D(\vec{k}_{12},\vec{r}_{12})=\sum_l\,d_l, \tag{13}$$

with

$$\begin{aligned}d_l(\vec{k}_{12},\vec{r}_{12})=&\exp(-\pi\eta_{12}/2)\Gamma(1-i\eta_{12})\\&\times\frac{(-is_{12})^l\Gamma(l+i\eta_{12})}{\Gamma(i\eta_{12})\cdot(2l-1)!!l\cdot!}\\&\times P_l(\gamma_{12})\,{}_1F_1(l+i\eta_{12};2l+2;-2is_{12}).\end{aligned} \tag{14}$$

In the special case of the monopole term ($l=0$) we get

$$\begin{aligned}d_0(k_{12},r_{12})=&\exp(-\pi\eta_{12}/2)\Gamma(1-i\eta_{12})\\&\times\,{}_1F_1(i\eta_{12};2;-2is_{12}),\end{aligned} \tag{15}$$

and for the dipole term ($l=1$)

$$\begin{aligned}d_1=&\exp(-\pi\eta_{12}/2)\Gamma(1-i\eta_{12})\frac{r_{12}}{2}\\&\times P_1(\gamma_{12})\;{}_1F_1[1+i\eta_{12};4;-2is_{12}].\end{aligned} \tag{16}$$

Since the Hylleraas function as well as the distortion factor depend explicitly on the coordinate r_{12}, we expand the product of the initial state and each partial-wave term of the distortion factor in terms of partial waves as

$$\begin{aligned}&\Psi_0(r_1,r_2,r_{12})\;{}_1F_1[l+i\eta_{12};2l+2;-2ik_{12}r_{12}]\\&\quad=\sum_{l'}\,\psi_{ll'}(r_1,r_2)P_{l'}(\cos\theta_{12}),\end{aligned} \tag{17}$$

where

$$\begin{aligned}\psi_{ll'}(r_1,r_2)=&\int_{-1}^1 du\Psi_0(r_1,r_2,r_{12}(u))\\&\times\,{}_1F_1[l+i\eta_{12};2l+2;-2ik_{12}r_{12}(u)]P_{l'}(u)\end{aligned} \tag{18}$$

and $r_{12}(u)=\sqrt{r_1^2+r_2^2-2r_1r_2u}$.

This partial-wave expansion in the relative angular momentum conjugate to the angle γ_{12} is then converted into a partial-wave expansion of single-particle angular momenta. For example, in the case of one electron remaining bound (excitation ionization) we have $\vec{k}_{12}=\frac{1}{2}\vec{k}_1$ and

$$\begin{aligned}s_{12}^l P_l(\gamma_{12})=&\frac{4\pi}{2l+1}\sum_{m=-l}^{l}k_{12}^l Y_{lm}^*(\hat{k}_{12})r_{12}^l Y_{lm}(\hat{r}_{12})\\=&\frac{4\pi}{2l+1}\sum_{m=-l}^{l}(k_1/2)^l Y_{lm}^*(\hat{k}_1)\end{aligned} \tag{19}$$

$$\begin{aligned}&\times\sum_{j_1=0,j_1+j_2=l}r_1^{j_1}r_2^{j_2}\sqrt{\frac{4\pi(2l+1)!}{(2j_1+1)!(2j_2+1)!}}\\&\times Y_{j_1j_2lm}(\hat{r}_1,\hat{r}_2).\end{aligned} \tag{20}$$

For the double continuum, a similar expansion of $\vec{k}_{12}$ is performed. In Eq. (20) $Y_{j_1j_2lm}$ are the bipolar spherical harmonics.

In the numerical results to be presented below we have included partial waves for the ''fast'' electron up to $l_1=30$ while for the slow electron we have terminated the expansion at $l_2=6$. In our evaluation we have used a discrete pseudostate expansion for the slow electron (for double ionization) or bound states (for excitation ionization) as discussed in [6]. Within the state space of pseudostates, the Rydberg series of $He^+(n)$ is represented by typically the ten lowest pseudostates while the remainder (typically of the order 30) are associated with continuum states. Because of the discretization of the spectrum, the borderline between excitation, excitation ionization, and double ionization is therefore only defined to within the cross section of ± 1 pseudostates (the highest bound vs the lowest continuum state). Since the double ionization cross section is only a small fraction of the excitation-ionization cross section (of the order of $\approx 1\%$), the discretization therefore introduces an error of a few percent.

III. EXPERIMENT

A. Experimental setup

The experiment was done at the high-energy photon beam line ID15A at ESRF in Grenoble [25]. Radiation from both an asymmetric multipole wiggler with a critical energy of 44 keV and a superconducting wavelength shifter with a critical energy of 100 keV was monochromatized using a single horizontally focusing Laue-type bent Si crystal. The monochromator was located at a distance of about 55 m from the sources and the x-ray beam size on the monochromator was 34.0×5.9 mm^2. The crystal was bent so that the x-ray beam was focused on the target at a distance of 8 m from the monochromator.

Three different energies were selected for the experiment. To keep the setup at a fixed Bragg angle, three reflections from different crystals were used: Si 111, 311, and 331 corresponding to the energies 38.86, 74.41, and 97.80 keV, respectively. The asymmetric cut and the thickness of each crystal were optimized to maximize the flux. In Table I the energies, bandwidths, flux, bending radii, thicknesses, and asymmetric cuts of the crystals are shown. The flux is normalized to 100 mA electron beam current.

At 38.85 keV the photon beam contained to about 21% photons from the third order reflection at 116.55 keV and about 7% from the fourth order reflection at 155.4 keV. The second order reflection was forbidden from the crystal geometry. Thus an influence of a high-energy R_C, which can be different from the main value at 38.85 keV, cannot be excluded, although it is expected to be a small effect. A discussion of such an effect will be given with the experimental results. At the energies of 74.41 and 97.80 keV, no significant contributions from higher-order reflections were contained in the beam, as they were strongly suppressed by the flux of the source at those energies.

TABLE I. The energies, bandwidths, fluxes, asymmetry cuts, bending radii, and thicknesses of the Si crystals used.

hkl	E_γ (keV)	ΔE_γ (keV)	Flux (counts/sec)	$\chi(^\circ)$	ρ (m)	t (mm)
111	38.86	1.98	4.2×10^{13}	35.26	-21.6	2
311	74.41	3.61	3.8×10^{13}	7.24	-18.5	5
331	97.80	4.76	2.7×10^{13}	13.26	-18.7	5

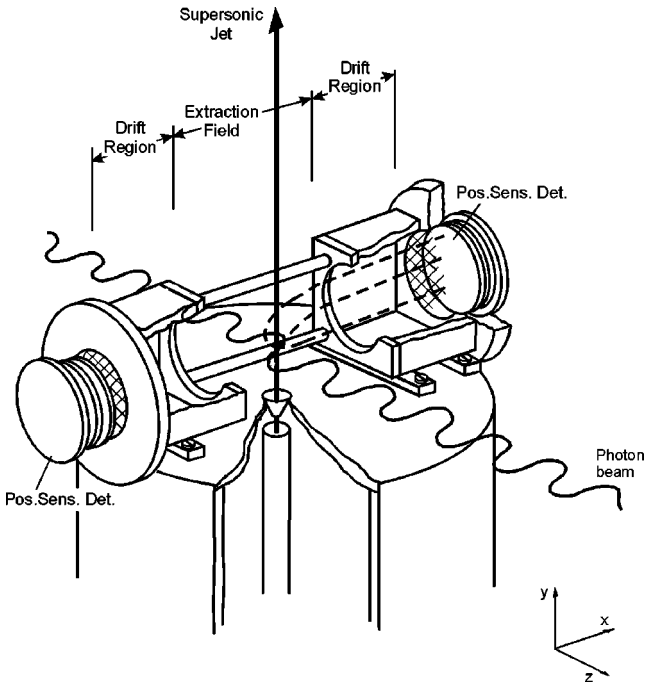

FIG. 1. Sketch of the double COLTRIMS spectrometer. The position-sensitive channel-plate detectors are equipped with wedge-and-strip readout, the ion time of flight is determined with respect to the beam pulse. Both spectrometer halves were successively used for ion detection with appropriate directions of the extraction field.

The photon beam was collimated to 2-mm width and 4-mm height by means of two sets of tungsten four-jaw slits, 0.55 m and 0.95 m upstream of the target. It entered into the experimental chamber through a 0.5 mm thick Be window. A magnet with an inhomogeneous field of up to 180 G was placed right behind the entrance window to prevent secondary electrons produced in the window from reaching the target area. The beam was intersected with a cold (<1 K) supersonic helium jet with a density of 5×10^{12} atoms/cm^2 and a diameter of 2.5 mm. The background pressure was 1×10^{-7} mbar.

The target volume was placed in the area of a homogeneous electrostatic field, which projected the ions onto a position sensitive channel plate detector (PSCD) with wedge-and-strip anode readout (COLTRIMS ion spectrometer). This spectrometer will be described in more detail later.

The beam left the chamber through a 0.5-mm-thick Be window located 0.87 m downstream from the target, and was dumped behind collimating lead bricks to shield against secondary particles created at the beam dump.

The experiment was performed during the 16-bunch mode of the ESRF, which corresponds to 176-nsec time difference between successive beam pulses. The time-of-flight (TOF) of the ions was measured with respect to the pulse reference signal delivered by the storage ring. As the ion TOF was in the range of a few μsec, the full TOF distribution was ''wrapped around'': the full TOF was cut into parts of 176-nsec length which were summed up in a spectrum of this length. The position signals, pulse height, and the TOF spec-

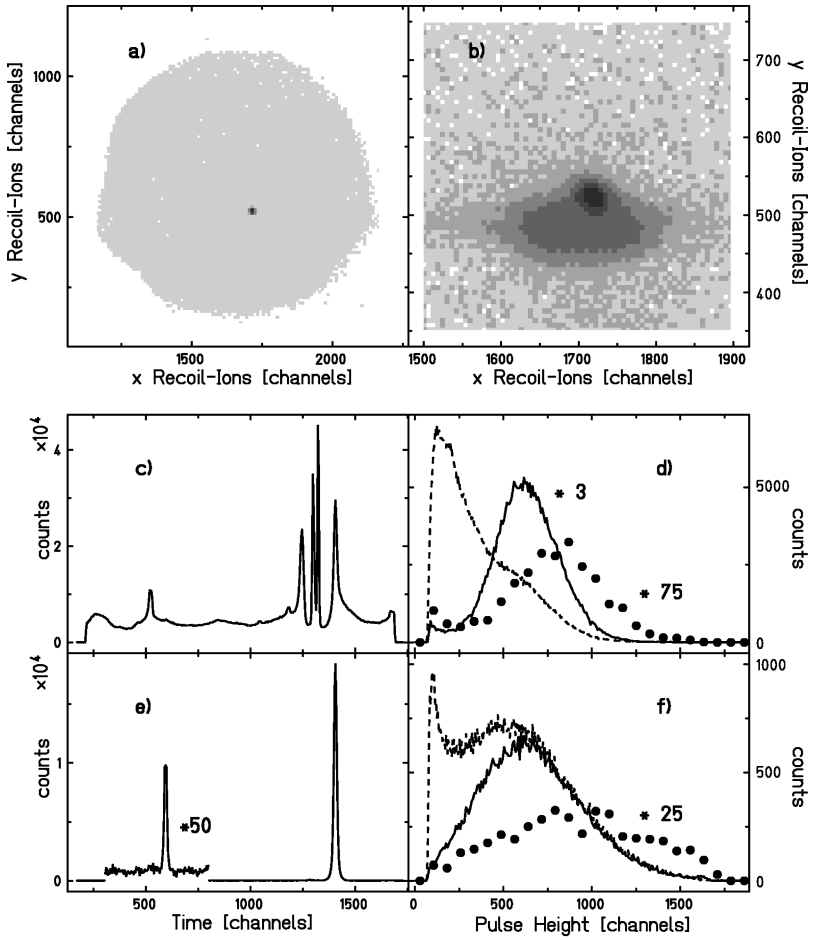

FIG. 2. Recoil-ion position distribution taken with lens spectrometer for the complete detector in a linear intensity scale (a) and for an enlarged area around the target in a log scale (b). The target volume is focused into the round spot, the ions created in ionization of the residual gas are focused into the lower diffuse spot. (c), (e) Time-of-flight distributions before and after background reduction (see text). The part around the He^{2+} peak was multiplied by 50. Detector pulse height distributions before (dashed line) and after background reduction for the *z*-stack detector (d) and the chevron detector (f). The background-reduced distributions for the He^{+} charge state are given in solid lines, for the He^{2+} charge state in filled circles. They were multiplied by 3 and 75 (d) and 25 (f), respectively. The data were taken at $E_\gamma = 80$ keV.

trum were recorded in ''list mode,'' allowing for an event-by-event off-line correlation between these quantities.

The COLTRIMS spectrometer used here was designed for the coincident detection of the recoiling ion and an electron resulting from a Compton process. Therefore it was a combination of two independent spectrometers and detectors with a common extraction field (in *x* direction) directed perpendicular to the photon and gas beams (*z* and *y* direction, respectively). This geometry is schematically shown in Fig. 1. One spectrometer (in the following called ''homogeneous field spectrometer'') was built in a Wiley-McLaren geometry [26] with an acceleration region of length $s_e = 4.5$ cm and a drift path of $2 \times s_e = 9$ cm to ensure a TOF focusing of particles which started at different *x* positions into one common time of flight. The opposite spectrometer (in the following called ''lens spectrometer'') was equipped with a sudden potential step within the acceleration field, which provides a focusing of different starting positions of the particle trajectories in the *y*-*z* plane into one common detection position, in addition to the TOF focusing [27]. Both the TOF and position focusing are in first order independent of the ion's initial momentum. The lens spectrometer was equipped with a double channel plate detector in chevron geometry with a total voltage of 1950 V over the channel plates, the homogeneous field spectrometer with a triple channel plate *z*-stack detector, operated with 2500 V overall voltage. In this work, these two COLTRIMS spectrometers were used for ion detection only, to perform two independent measurements of R_C in successively applying appropriate directions of the extraction field.

B. Data analysis

The data were recorded with a low discrimination threshold to ensure the maximal ion detection efficiency. Therefore the raw spectra contain to a large amount background events due to the detection of scattered photons or noise from electromagnetic signals from the environment, resulting in a non-clear TOF structure as displayed in Fig. 2(c). In addition, this background leads to a pulse height distribution which decays practically exponentially from threshold. The dashed lines in Figs. 2(d) and 2(f) show this distribution for both detectors,

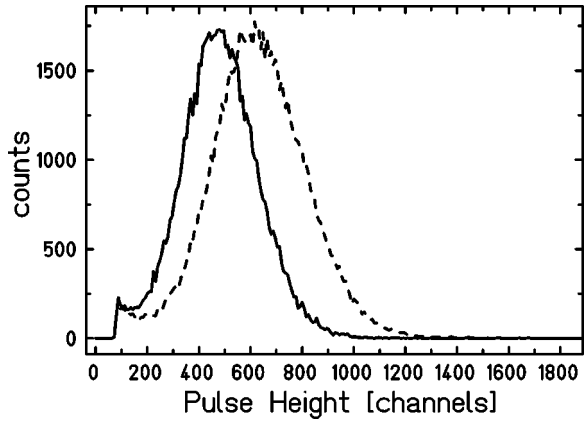

FIG. 3. Pulse height distribution for He^+ ions detected with the *z*-stack detector operated at 2500 V total amplification voltage. The preacceleration for the ions before hitting the channel plate was 2500 V (dashed line) and 1250 V (solid line). Both distributions are normalized to an identical maximum value.

with the homogeneous field spectrometer (*z*-stack detector) having a considerably larger background contamination [Fig. 2(d)]. The TOF spectrum in Fig. 2(c) was taken with the homogeneous field spectrometer, corresponding to Figs. 2(d). The position distribution taken with the lens spectrometer is displayed in Figs. 2(a) and 2(b). Here, the target volume given by the overlap region of the photon and gas beams is focused into a spot of about 2×2 mm^2 which is offset in the positive *y* direction by the supersonic jet momentum of 5.9 a.u. The ions created in the residual gas along the photon beam are focused into the diffuse lower spot. In using the benefits of this well localized target area, the position sensitivity of the imaging detector, and the list-mode data procedure, a highly efficient off-line background reduction can be performed in selecting only a small window around the jet area on the position sensitive recoil ion detector for further analysis. In this way, the background events outside the target volume are excluded in a controlled manner. As a verification of this background reduction, the pulse height distribution, shown in Figs. 2(d) and 2(f) for the He^+ charge state (solid lines) and for the He^{2+} charge state (filled circles), now exhibits a narrow peak as a response of the *z*-stack detector to the ions, and a broader distribution for the chevron detector. In both cases the pulse height distribution for both helium charge states is well separated from the threshold at low pulse heights and the overflow at high pulses. The TOF distribution after background reduction, shown in Fig. 2(e), now clearly shows the peaks of both helium charge states. Here, as for the rest of the data analysis, a selection of 2×2 mm^2 for the lens spectrometer and 9×9 mm^2 for the homogeneous field spectrometer were used. This window fully encloses the target spot. The data analysis procedure was carried out for the independent data sets taken with the two spectrometers, yielding two fully independent values of R_C at one photon energy. For $E_\gamma = 97.80$ keV, only one measurement with the homogeneous field spectrometer was made.

The characteristics of the COLTRIMS method ensure an identical collection efficiency of both He charge states due to identical solid angles, since the well localized target produced by the the supersonic jet in combination with the large extraction field results in a full 4π collection of all He ions, independent of their charge state. This is verified in imaging the target by the position sensitive detector: no He ionization was observed outside the target position. Furthermore, a secondary charge exchange of the He ions created in the Compton process in collisions with the residual gas particles can be excluded by the low target chamber pressure outside the target volume.

Additionally, different cross checks were made to control further possible systematic errors in the measurement of R_C.

(a) Independent sets of measurements were taken with 2500 V and 1250 V preacceleration projecting the ions onto the *z*-stack detector (homogeneous field spectrometer) while keeping the overall detector voltage constant. In this way, R_C is checked against a possible influence of the detection efficiency on the different impact velocities of both He charge states on the detector. The resulting pulse height distributions for the He^+ charge state are displayed in Fig. 3. Both preaccelerations yield the same width of the pulse height distribution relative to its center position, with the latter being shifted by 150 channels towards lower pulse heights for the lower preacceleration. It is well separated from the threshold, still, and no difference in the resulting R_C could be observed. This demonstrates that the measurements were made in a detection regime which ensures an equal detection efficiency for both helium charge states. The data presented here were taken with the larger preacceleration voltage.

(b) Complementarily, at a fixed preacceleration value several lower ''software thresholds'' have been applied in the data analysis. The resulting deviation of R_C from the zero-threshold value $(R_C)_0$ is displayed for both detectors in Table II. The threshold value used is given in relative units [analog-to-digital converter (ADC) channels], corresponding to the pulse height distributions given in Figs. 2(d) and 2(f). The result demonstrates a clear independence of R_C for a significantly extended range of lower thresholds. This indicates that within this range the detector response was identical for both helium charge states. Therefore the loss of counts due to the threshold is identical for both charge states. The final results for R_C were extracted for a zero software

TABLE II. Deviation of R_C at $E_\gamma = 80$ keV as a function of a lower ''software threshold'' on the detector pulse height. Given is the value $[R_C-(R_C)_0]$, the threshold value in ADC channels, corresponding to the pulse height distributions given in Figs. 2(d) and 2(f). The results for R_C given in Table III were extracted at 0 threshold.

Threshold (channels):	0	100	200	300	350	400	425	450
z stack:	0.00	0.00	0.00	+0.01	+0.03	+0.05	+0.07	+0.10
Chevron:	0.00	0.00	+0.01	+0.04	+0.07	+0.12	+0.14	+0.16

TABLE III. Experimental results.

E_γ (keV)	R_C (%) (homogeneous field spectrometer)	R_C (%) (lens spectrometer)
38.86	0.98 ± 0.04	0.98 ± 0.1
74.41	0.94 ± 0.04	0.93 ± 0.05
97.80	0.98 ± 0.09	

threshold. As a consequence, any influence of different pulse height distributions for both charge states on R_C can be excluded. The increase of R_C towards larger software thresholds demonstrates a larger loss of He^+ compared to the He^{2+} events, as the pulse height distribution is centered at slightly larger values for the He^{2+} charge state [see Figs. 2(d) and 2(f)]. This effect is larger for the chevron detector (lens spectrometer) which shows the broader pulse height distribution. This is a clear demonstration of the possible influence on experimental values of R by a detection threshold, which, however, can clearly be excluded only by the data acquisition and data analysis methods applied here.

(c) Data were taken with the magnet at the entrance window both switched on and switched off. No change in the ion production rate and in R_C could be observed, excluding any observable influence of secondary electrons produced in the entrance window on the total ionization rate.

(d) More strongly, ionization due to secondary particles either entering through the entrance window or produced in the experimental chamber, such as stray photons, secondary low-energy photons, or secondary charged particles, is not restricted to the well defined photon beam position. As a result, He ionization would have to occur along an extended region of the gas jet. No He ions could be observed outside the target beam spot defined by the overlap of gas jet and photon beam, strictly excluding any ionization due to secondary particles.

(e) The photon energy distribution was measured with a Ge detector in analyzing Compton backscattered photons from the entrance window. For all three photon energies no contribution of photons of an energy lower than the main energy could be found. This observation excludes any influence of ionization due to Compton scattering of lower-energy photons traveling with the beam than the main energy. This method is significant down to a photon energy in the range of 10 keV, as absorption of the scattered photons in the air and the detector window is increasing with decreasing photon energy.

(f) Photons traveling with the beam of an energy below 10 keV would lead to a significant contribution of ionization from photoabsorption. This process is characterized by a well defined recoil-ion momentum, compensating for the photoelectron momentum [28]. Since the deviation of the recoil-ion detection position from its center is proportional to its momentum and therefore proportional to the absorbed photon energy, the small acceptance window for the recoil-ion position in the data analysis excludes photoabsorption events for photons above a given energy. For the lens spectrometer the window is equivalent to an acceptance of He^+ ions with a momentum in the y-z plane up to 3.3 a.u., discriminating against photoabsorption events with $E_\gamma > 200$ eV. A possible contamination of such low-energy photons in the main beam cannot enter into the target chamber as they are completely filtered out by the entrance window. For the homogeneous field spectrometer, due to the large target size on the detector, the window corresponds to an acceptance of a larger He^+ momentum of 17 a.u. in the y-z plane.

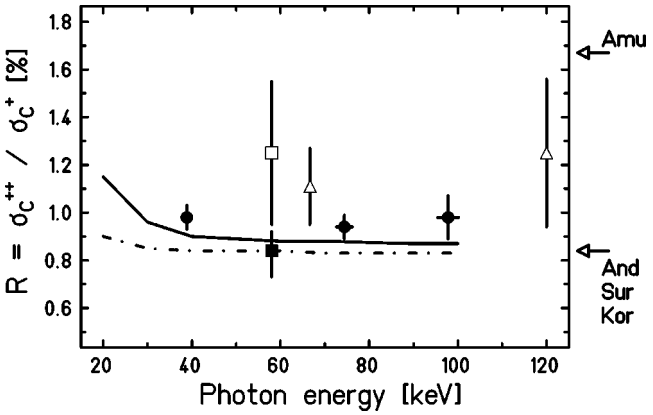

FIG. 4. Ratio of double to single ionization after Compton scattering. This experiment, solid circles; this calculation, solid line ($3C$) and dash-dotted line ($2C$). Other experimental values: solid square, Spielberger *et al.* [35]; open triangles, Becker *et al.* [12]; open square, Wehlitz *et al.* [36]. Arrows, calculated values of R_C^∞: Andersson and Burgdörfer (And) [8]; Surić *et al.* (Sur) [9]; Kornberg and Miraglia (Kor) [10]; Amusia and Mikhailov (Amu) [11].

(g) At $E_\gamma = 100$ keV, data were taken without the He target during about 1/3 of the experimental time with He. No peak structure could be observed at the He^{2+} TOF position, ensuring that no possible contribution of H_2^+ ionization from the residual gas was contaminating the experiment.

IV. RESULTS AND DISCUSSIONS

The experimental results are given in Table III and displayed together with the calculations in Fig. 4. With the exception of the value for the lens spectrometer at $E_\gamma \approx 40$ keV, where the statistics was comparatively poor, the remaining error bars are dominated to equal parts by statistics and the subtraction of the remaining background after the off-line data analysis procedure.

Within the range of photon energies of $40 \leqslant \hbar\omega \leqslant 100$ keV investigated, the ratio R_C is not found to be significantly energy dependent. Within the error bars, our data are consistent with the earlier measurement at 58 keV of $R_C \approx 0.85$. Our data are in agreement with the values reported by Becker *et al.* [12], although the center values are systematically lower by about 30%. The latter data have significantly larger error bars. Both the $2C$ and the $3C$ calculations reproduce the weak energy dependence of the data. The $3C$ calculation gives consistently higher values than the $2C$ calculation for the ratio and therefore shows a better agreement with the data.

At $E_\gamma \approx 40$ keV our experimental value is given. As in the photon beam the third-order reflection was contained to 21% and the fourth to 7%, the possible differences of the ''true'' values of R_C at $E_\gamma = 116.55$ keV, $\Delta R(117)$, and at E_γ

$=155.4$ keV, $\Delta R(155)$, to the ''true'' value at $E_\gamma = 38.85$ keV, $R(38.95)$, lead to a change of our experimental value $R^{40}_{\rm expt}$ according to

$$R^{40}_{\rm expt} = R(38.95) + 0.05\,\Delta R(155) + 0.19\,\Delta R(117). \quad (21)$$

Here, the decrease of the total Compton scattering cross section was taken into account [30]. As from the calculations both $\Delta R(117)$ and $\Delta R(155)$ are expected to be smaller than 0.04%, the resulting correction to the experimental value would be on the order of $\Delta R < 0.01\%$, which is small compared to the error bars.

We interpret our finding of a practically constant R_C significantly higher than $R_C^\infty = 0.84$ as an indication of a very slow convergence towards the asymptotic value. Thus the influence of final-state correlations seems to persist up to high photon energies. This can be understood since the energy transfers in the Compton scattering process show a broad distribution. As discussed above, even at $\hbar\omega = 100$ keV, a considerable fraction of the double ionization cross section is associated with two-electron final states with a two-electron energy of only a few keV. For the latter, electron-electron correlations during the collision and in the final state are known to be important from corresponding photoabsorption data leading to an increase of the ratio by up to a factor 2. The low-energy tail of the energy transfer distribution also limits the accuracy of our calculations.

Although within this picture R_C is well understood in the energy regime investigated here, the behavior of R_C at larger energies still remains of interest. Due to the slow convergence to R_C^∞, such an investigation has to be done at photon energies significantly larger than the highest energy used here. At higher energies, however, relativistic effects in Compton scattering as well as pair production above 1.02 MeV may become increasingly important. It is not clear that R_C remains unchanged in the relativistic regime. As the available photon flux is decreasing with increasing energy such an experimental work seems to be beyond the capability of today's synchrotron radiation facilities. More promising is an investigation of R_C as a function of the photon energy transfer, where the different regimes from large energy transfer, which should be equivalent to the asymptotic regime, down to small energy transfer, can be studied separately. Such an experiment requires an angular resolved detection of the scattered photon coincident to the ion detection. Complementarily, a momentum analysis of the emitted electrons in coincidence to the ion yields the same information. In a first attempt to achieve this aim, a coincident momentum determination of one emitted electron and the recoiling ion was done in the same beam time in which this work has been carried out. We plan to publish the results in the future.

Our results permit an interesting comparison with very recent data for charged-particle collisions. The quantum amplitudes for both Compton scattering and scattering by fast charged particles are proportional to the atomic scattering factor $\langle f|e^{i\vec{k}_f\cdot\vec{r}}|i\rangle$. This means that Compton scattering data can be directly compared with data for fast charged particles [13,31,32] under the condition that the first Born approximation is valid for both processes and that the energy transfer is large. In particular, the ratio of double to single ionization for Compton scattering may be compared to that for charged particles. Recent measurements of Cocke and co-workers [33] at 4, 5, and 10 MeV proton collisions have yielded values of 1.34%, 1.28%, and 1.2%, respectively. These numbers are systematically higher than ours by $\approx 30\%$. The origin of this discrepancy is not yet understood. One possible origin lies in the slow convergence to the perturbative limit for charged-particle collisions as a function of the transferred energy. Note that the equivalence of the charged-particle ratio and the ratio for Compton scattering requires that the final-state interaction with the projectile is entirely negligible. Under the kinematic conditions of the charged-particle experiment [33], where the double ionization is initiated by a binary-encounter collision, the projectile propagates ''in between'' the slow and the fast electron in both momentum and coordinate space. It is therefore expected to perturb the final-state correlation between the two electrons even at high velocities. While this effect should be small at sufficiently high energies, it may not be negligible at the energies investigated in [33]. We also note that the earlier experiment by Wu *et al.* [34] probes a different kinematic region yielding ratios in closer agreement with the present data, however, with a much larger error bar. More experimental and theoretical work appears to be necessary to unravel the relationship between these different experimental data sets.

ACKNOWLEDGMENTS

This work was supported in part by the DFG, BMBF, DAAD, NSF, and by U.S. DOE Office of Basic Energy Sciences under Contract No. DE-AC05-96OR22464 with ORNL managed by LMERC, Max-Planck-Forschungspreis, EC. H.B. gratefully acknowledges support from the Alexander v. Humboldt Foundation, R.D. gratefully acknowledges support from the Habilitanden Programm of the DFG. We gratefully acknowledge the support of the University of Frankfurt in the transportation of the experimental setup to ESRF, Grenoble, in particular to Ch. Kazamias and W. Schäfer. We are grateful to U. Becker for communication of his unpublished results.

[1] J.H. McGuire, *Electron Correlation Dynamics in Atomic Collisions* (Cambridge University Press, Cambridge, England, 1997).

[2] F.W. Byron and C.J. Joachain, Phys. Rev. **164**, 1 (1967).

[3] T. Åberg, Phys. Rev. A **A2**, 1726 (1970).

[4] A. Dalgarno and H.R. Sadeghpour, Phys. Rev. A **46**, R3591 (1992).

[5] L. Spielberger, O. Jagutzki, R. Dörner, J. Ullrich, U. Meyer, V. Mergel, M. Unverzagt, M. Damrau, T. Vogt, I. Ali, Kh. Khayyat, D. Bahr, H.G. Schmidt, R. Frahm, and H. Schmidt-

Böcking, Phys. Rev. Lett. **74**, 4615 (1995).
[6] Y. Qiu, J.Z. Tang, and J. Burgdörfer, Phys. Rev. A **57**, R1489 (1998).
[7] L.R. Andersson and J. Burgdörfer, Phys. Rev. Lett. **71**, 50 (1993).
[8] L.R. Andersson and J. Burgdörfer, Phys. Rev. A **50**, R2810 (1994).
[9] T. Surić, K. Pisk, B.A. Logan, and R.H. Pratt, Phys. Rev. Lett. **73**, 790 (1994).
[10] M.A. Kornberg and J.E. Miraglia, Phys. Rev. A **53**, R3709 (1996).
[11] M. Ya Amusia and A.I. Mikhailov, J. Phys. B **28**, 1723 (1995); Phys. Lett. A **199**, 209 (1995).
[12] U. Becker, G. Prümper, J. Viefhaus, M. Wiedenhöft, C. J. Levin, and I. A. Sellin, Aust. J. Phys. (to be published).
[13] J. Burgdörfer, L.R. Andersson, J.H. McGuire, and T. Ishihara, Phys. Rev. A **50**, 349 (1994).
[14] J. Ullrich, R. Moshammer, R. Dörner, O. Jagutzki, V. Mergel, H. Schmidt-Böcking, and L. Spielberger, J. Phys. B **30**, 2917 (1997).
[15] L. Spielberger, O. Jagutzki, R. Dörner, V. Mergel, U. Meyer, Kh. Khayyat, T. Vogt, M. Achler, H. Schmidt-Böcking, J. Ullrich, M. Unverzagt, B. Krässig, M. Jung, E.P. Kanter, D.S. Gemmell, M.H. Prior, H. Khemliche, and C.L. Cocke, in *Applications of Accelerators in Research and Industry*, edited by J. L. Duggan and I. L. Morgan, AIP Conf. Proc. 392 (AIP, Woodbury, NY, 1997), p. 213.
[16] R. Dörner, T. Vogt, V. Mergel, H. Khemliche, S. Kravis, C.L. Cocke, J. Ullrich, M. Unverzagt, L. Spielberger, M. Damrau, O. Jagutzki, I. Ali, B. Weaver, K. Ullmann, C.C. Hsu, M. Jung, E.P. Kanter, B. Sonntag, M.H. Prior, E. Rotenberg, J. Denlinger, T. Warwick, S.T. Manson, and H. Schmidt-Böcking, Phys. Rev. Lett. **76**, 2654 (1996).
[17] G. Baym, *Lectures on Quantum Mechanics* (Addison-Wesley, New York, 1974).
[18] W. Heitler, *The Quantum Theory of Radiation* (Oxford University Press, London, 1954).
[19] T. Åberg and J. Tulkki, in *Atomic Inner-shell Processes*, edited by B. Crasemann (Plenum Press, New York, 1985), p. 415.
[20] V.A. Fock, Izv. Akad. Nauk SSSR, Ser. Fiz. **18**, 161 (1954).
[21] L. Pekeris, Phys. Rev. **5**, 1649 (1958).
[22] L. Vainshtein, L. Presnyakov, and I. Sobelman, Zh. Éksp. Teor. Fiz. **45**, 2015 (1963); Sov. Phys. JETP **18**, 1383 (1964).
[23] M. Brauner, J.S. Briggs, and H. Klar, J. Phys. B **22**, 2265 (1989).
[24] J. Wang, J.H. McGuire, J. Burgdörfer, and Y. Qiu, Phys. Rev. Lett. **77**, 1723 (1996).
[25] Th. Tschentscher and P. Suortti, J. Synchrotron Radiat. **5**, 286 (1998).
[26] W.C. Wiley and I.H. McLaren, Rev. Sci. Instrum. **26**, 1150 (1955).
[27] V. Mergel, *Dynamische Elektronenkorrelationen in Helium* (Shaker Verlag, Aachen, Germany, 1996); R. Dörner, V. Mergel, L. Spielberger, M. Achler, Kh. Khayyat, T. Vogt, H. Bräuning, O. Jagutzki, T. Weber, J. Ullrich, R. Moshammer, M. Unverzagt, W. Schmitt, H. Khemliche, M.H. Prior, C.L. Cocke, J. Feagin, R.E. Olson, and H. Schmidt-Böcking, Nucl. Instrum. Methods Phys. Res. B **127**, 225 (1997).
[28] Due to small photon momentum and the three-body nature of the photoabsorption process it is strictly the ion which has to compensate for the momentum of the photoelectron. In contrast, due to the two-body scattering at the electron in the Compton process, here ions with a momentum distribution around zero with a width given by the Compton profile are expected [5,29].
[29] L. Spielberger, O. Jagutzki, R. Dörner, J. Ullrich, U. Meyer, V. Mergel, M. Unverzagt, M. Damrau, T. Vogt, I. Ali, Kh. Khayyat, D. Bahr, H.G. Schmidt, R. Frahm, and H. Schmidt-Böcking, in *The Physics of Electronic and Atomic Collisions: XIX International Conference*, edited by L.J. Dubé, J.B.A. Mitchell, J.W. McConkey, and C.E. Brion, AIP Conf. Proc. 360 (AIP, New York, 1995), p. 773.
[30] E. Storm and H.I. Israel, Nucl. Data, Sect. A **7**, 565 (1970).
[31] J. Burgdörfer, Y.T. Qiu, J. Wang, and J.H. McGuire, in *X-Ray and Inner-Shell Processes, 17th International Conference*, edited by R.L. Johnson, AIP Conf. Proc. 389 (AIP, New York, 1996), p. 475.
[32] J. Wang, J.H. McGuire, and J. Burgdörfer, Phys. Rev. A **54**, 613 (1996).
[33] W.R. DeHaven, C. Dilley, A. Landers, E.Y. Kamber, and C.L. Cocke, Phys. Rev. A **57**, 292 (1998).
[34] W. Wu, S. Datz, N.L. Jones, H.F. Krause, B. Rosner, K.D. Sorge, and C.R. Vane, Phys. Rev. Lett. **76**, 4324 (1996).
[35] L. Spielberger, O. Jagutzki, B. Krässig, U. Meyer, Kh. Khayyat, V. Mergel, Th. Tschentscher, Th. Buslaps, H. Bräuning, R. Dörner, T. Vogt, M. Achler, J. Ullrich, D.S. Gemmel, and H. Schmidt-Böcking, Phys. Rev. Lett. **76**, 4685 (1996).
[36] R. Wehlitz, R. Hentges, G. Prümper, A. Farhat, T. Buslaps, N. Berrah, J.C. Levin, I.A. Sellin, and U. Becker, Phys. Rev. A **53**, R3720 (1996).